Optics Letters

Dispersive-wave-based octave-spanning supercontinuum generation in InGaP membrane waveguides on a silicon substrate

Utsav D. Dave,[1,2,*] Charles Ciret,[3] Simon-Pierre Gorza,[3] Sylvain Combrie,[4] Alfredo De Rossi,[4] Fabrice Raineri,[5,6] Gunther Roelkens,[1,2] and Bart Kuyken[1,2]

[1]Photonics Research Group, Department of Information Technology, Ghent University-IMEC, Ghent B-9000, Belgium
[2]Center for Nano- and Biophotonics (NB-photonics), Ghent University, Ghent, Belgium
[3]OPERA-Photonique, Université Libre de Bruxelles (ULB), 50 Av. F. D. Roosevelt, CP 194/5, B-1050 Bruxelles, Belgium
[4]Thales Research and Technology, Route Départementale 128, 91767 Palaiseau, France
[5]Laboratoire de Photonique et de Nanostructures, CNRS-UPR20, Route de Nozay, 91460 Marcoussis, France
[6]Université Paris Denis Diderot, 75205 Paris, France
*Corresponding author: utsav.dave@intec.ugent.be

Received 22 June 2015; accepted 3 July 2015; posted 8 July 2015 (Doc. ID 243304); published 27 July 2015

We demonstrate the generation of an octave-spanning supercontinuum in InGaP membrane waveguides on a silicon substrate pumped by a 1550-nm femtosecond source. The broadband nature of the supercontinuum in these dispersion-engineered high-index-contrast waveguides is enabled by dispersive wave generation on both sides of the pump as well as by the low nonlinear losses inherent to the material. We also measure the coherence properties of the output spectra close to the pump wavelength and find that the supercontinuum is highly coherent at least in this wavelength range.

OCIS codes: (320.6629) Supercontinuum generation; (190.4390) Nonlinear optics, integrated optics.

http://dx.doi.org/10.1364/OL.40.003584

In applications ranging from spectroscopy to telecommunications [1,2], supercontinuum sources with a broad bandwidth are desired. Recently, on-chip supercontinuum generation on a variety of waveguide platforms and targeting various wavelength ranges has become a subject of intensive research because of the potential of such sources to be compact, low cost, more efficient, and robust [3–7]. It is desirable that the pump source for generating the supercontinuum is located in a wavelength range where compact and efficient sources are readily available, like the telecommunications wavelength range. Moreover, for frequency-comb-based optical-frequency metrology, the stabilization of the frequency comb using the f–$2f$ self-referencing technique requires octave-spanning, coherent spectra [8]. We recently presented a new nonlinear platform based on highly nonlinear InGaP membrane waveguides bonded to a silicon substrate [9]. The large index contrast of this platform enables tight optical confinement for efficient nonlinear interactions and also allows for dispersion engineering. We also demonstrated that the waveguides did not suffer from the unwanted effects of two-photon absorption at 1550 nm owing to the large bandgap of InGaP. As such, the platform is well suited for on-chip supercontinuum generation. Since III-V materials also have large second-order nonlinear coefficients ($\chi^{(2)} =$ 110 pm/V [10]), it opens the possibility to do the f–$2f$ self-referencing to stabilize the optical frequency comb in an integrated platform. This new platform could thus offer a route to an on-chip carrier-envelope offset-stabilized comb source that could even be combined with on-chip mode-locked lasers. Here, we take the first step and demonstrate for the first time, to the best of our knowledge, the generation of an octave-spanning supercontinuum in a III-V-based platform on-chip. This was achieved by pumping 2-mm-long dispersion-engineered InGaP membrane waveguides with a femtosecond source centered around 1550 nm. The widest bandwidth obtained is 1.06 octaves wide at the −30 dB level relative to the pump. Since for several applications like the carrier offset stabilization of frequency combs, it is also important to preserve the coherence of the comb during supercontinuum generation, we also measured the coherence properties of the supercontinuum in a 200-nm spectral region near the pump and found that it is highly coherent.

The fabrication of the waveguide structures through bonding [9] allows for a high-index contrast between the III-V material and the SiO2/BCB bonding layer. A cross-section of such a waveguide, following the same fabrication procedure as in [9], is shown in the inset of Fig. 1. The waveguides have a fixed height of 250 nm, and the widths vary from 650 to 800 nm. It is well known that the dispersion properties of the waveguide play a critical role in broadband supercontinuum generation [11]. Here, we carefully tailored the dispersion

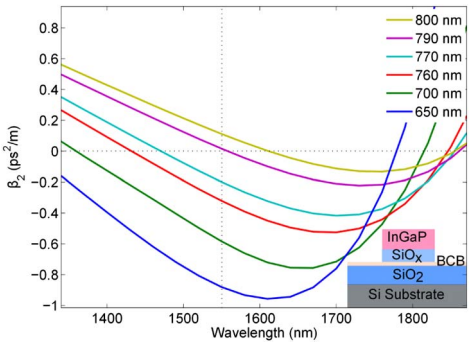

Fig. 1. Dispersion profiles of various InGaP waveguides used for the supercontinuum generation with zero dispersion wavelengths on both sides of the pump. Inset: schematic of the waveguide cross-section.

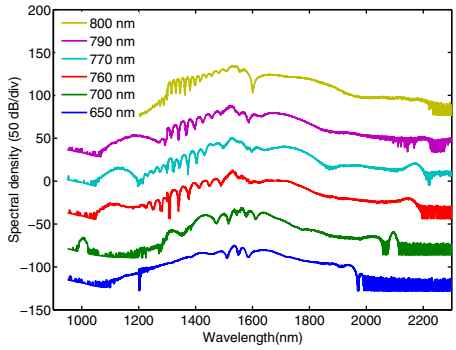

Fig. 2. Supercontinuum spectra at the output of the InGaP waveguides with varying widths—the spectra are displaced by 40 dB for clarity. The positions of the dispersive waves can be seen to shift with the width as expected. The spectra above and below the 1200-nm wavelength were measured with different optical spectrum analyzers with different noise floors.

properties of these waveguides to have anomalous dispersion at the pump wavelength and a zero dispersion wavelength (ZDW) on either side of the pump as shown in Fig. 1. For sufficiently high peak powers, the generation of dispersive waves on either side of the pump is thus expected. Knowing the dispersion properties of the waveguide, the spectral position of the dispersive waves can be calculated using Eq. (1) [12]:

$$\omega_{\mathrm{DW}} = \left[\beta(\omega_{\mathrm{DW}}) - \beta(\omega_S) + \frac{\omega_S}{\nu_{gs}} - (1 - f_R)\gamma P_S\right]\nu_{gs}. \quad \textbf{(1)}$$

Here, ω_{DW} and ω_S are the frequencies of the dispersive wave and the soliton pump, respectively, ν_{gs} is the group velocity at the pump wavelength, γ is the nonlinear parameter of the waveguide, P_S is the peak pump power, and f_R is the fractional Raman response that is assumed to be negligible here [13]. This equation shows that the dispersive wave is generated in the normal dispersion regime, i.e., on the other side of the ZDW with respect to the pump wavelength. As shown, for a given waveguide height, the positions of the ZDWs on either side of the pump at 1550 nm vary with the width. This feature thus enables one to tailor the position of the dispersive waves and hence the overall spectral properties of the supercontinuum. It should be noted that dispersive wave generation has been previously observed in InGaP photonic crystal waveguides [13].

For the supercontinuum-generation experiment, the pump was an optical parametric oscillator (OPO)-based femtosecond source centered at 1550 nm. The OPO delivers pulses with full width at half-maximum (FWHM) of 170 fs (as measured with an intensity autocorrelator) at a repetition rate of 82 MHz and an average power of 70–80 mW. The pulses were focused on a shallow etched grating coupler to interface with the InGaP membrane waveguide by means of a microscope objective. The outcoupling was done through a lensed fiber focused on the cleaved facet of the waveguide since the output spectrum is much wider than the grating coupler bandwidth. The resulting supercontinuum spectra for waveguides with different widths are shown in Fig. 2. The widest supercontinuum is observed for the 700-nm-wide waveguide, where we observe dispersive waves at 1005 and 2097 nm. Thus, the spectrum spans more than an octave of frequencies at a power level 30 dB below the output maximum power spectral density. As the waveguide's width increases, one can see that the blue (red) side dispersive waves move closer to (farther away from) the pump wavelength of 1550 nm, as expected from the ZDW moving closer to (farther away from) the pump.

In order to better understand the dynamics of the supercontinuum generation, we performed numerical simulations of the generalized nonlinear Schrodinger equation (GNLSE):

$$\frac{\partial E}{\partial z} = \sum_{k\geq 2}^{10} i^k \frac{\beta_k}{k!}\frac{\partial^k E}{\partial t^k} - \frac{\alpha}{2}E - \frac{\sigma}{2}(1 + i\mu)N_c E + \left(1 + \frac{i}{\omega_0}\frac{\partial}{\partial t}\right)\left(i\,\mathrm{Re}(\gamma)|E|^2 - \frac{\alpha_{3\mathrm{PA}}}{3A_{\mathrm{eff}}^2}|E|^4\right)E. \quad \textbf{(2)}$$

Here, β_k is the kth-order dispersion term calculated at the pump wavelength from a polynomial fit of the simulated effective index profile of the waveguide, α is the linear loss of the waveguide taken to be 12 dB/cm [9], ω_0 is central frequency, and γ is the nonlinear parameter whose value is taken to be 450 $\mathrm{W^{-1}\ m^{-1}}$ based on the previously reported value in [9] rescaled for the slightly larger calculated value of the effective area A_{eff} of the waveguide in question (0.21 $\mu\mathrm{m}^2$ for the 700×250 nm^2). Due to its large bandgap, the material does not suffer from two-photon absorption. However, we do include three-photon absorption (3PA) and the subsequent free carrier absorption and dispersion (FCA and FCD) in the GNLSE. These terms are defined, respectively, by the 3PA absorption coefficient $\alpha_{3\mathrm{PA}}$, the free-carrier-absorption cross-section σ, and free-carrier dispersion term μ. N_c represents the free-carrier density, which is obtained by solving the equation

$$\frac{\partial N_c}{\partial t} = \frac{\alpha_{3\mathrm{PA}}}{3\hbar\omega_0}\frac{|E|^6}{A_{\mathrm{eff}}^3} - \frac{N_c}{\tau_c}. \quad \textbf{(3)}$$

The value of the 3PA coefficient is taken to be 2.5×10^{-26} $\mathrm{m^3\ W^{-2}}$ as measured previously [9]. Values for the carrier lifetime τ_c (50 ps), the FCA ($\sigma = 7 \times 10^{-21}$ m^2), and the FCD ($\mu = 5.8$) coefficients are taken from the literature or extrapolated from similar materials [14–16]. Figure 3(a) shows the simulated supercontinuum (dotted line) after 2 mm of propagation length in the waveguide for a hyperbolic secant

input pulse with a FWHM of 170 fs and a peak power of 10 W. We can see that it matches reasonably well with the experimentally observed spectrum (solid line) and, in particular, the position of the dispersive waves on either side of the pump. Figure 3(b) shows the evolution of the spectrum as a function of the propagation length along the waveguide. One can see that the higher-order dispersion-mediated soliton fission followed by the dispersive wave generation on either side of the pump finally results in the observed spectrum. Only a small number of solitons are seen after propagation through the waveguide, as can be observed from Figs. 3(c) and 3(d), where the final temporal profile and the evolution along the waveguide are shown. Thus, a propagation length of 1.5 mm is enough to generate an octave-spanning supercontinuum, showing that highly compact devices are possible in this nonlinear platform. In contrast to previously reported supercontinuum generation in crystalline and hydrogenated amorphous silicon (spanning 0.56 and 0.53 octaves, respectively), we manage to achieve a much wider spectrum under similar experimental conditions [17,18]. Recently, an octave-spanning supercontinuum has been reported in silicon wire waveguides [19], but it requires much larger pulse energies than in our case (50 pJ and 2 pJ, respectively).

The buildup of the supercontinuum with increasing power of the input pulse is shown in Fig. 4. Experimentally, an attenuator was added before the input microscope objective in order to reduce the power without altering the pulse shape. The figure shows the comparison of the experimental and simulated buildup of the supercontinuum. One can see that overall, they agree very well. In the case of this waveguide, the dispersive waves appear on both sides of the pump simultaneously, which was also observed in the experiment. One can see that the dispersive wave generation occurs at a coupled peak power between 4 and 8 W, when the supercontinuum spectrum has

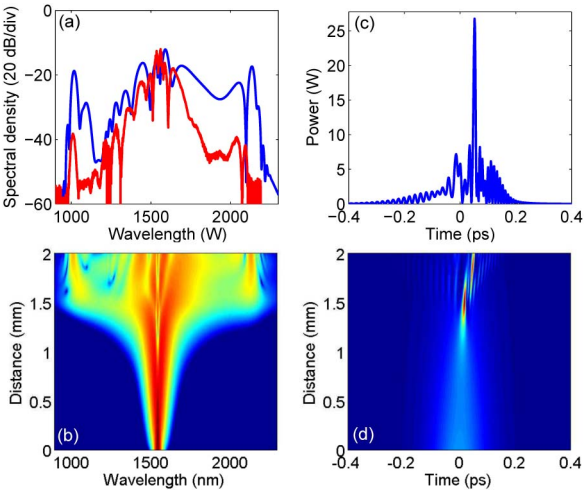

Fig. 3. Simulated (blue line) and experimental (red line) spectra at the output of the 700 × 250 nm waveguide. (b) The evolution of the supercontinuum spectrum over the propagation length of 2 mm showing the soliton fission and dispersive wave generation. (c) The simulated temporal profile of the supercontinuum showing a small number of solitons and the dispersive waves on the leading and trailing edges. (d) Evolution of the temporal profile with distance.

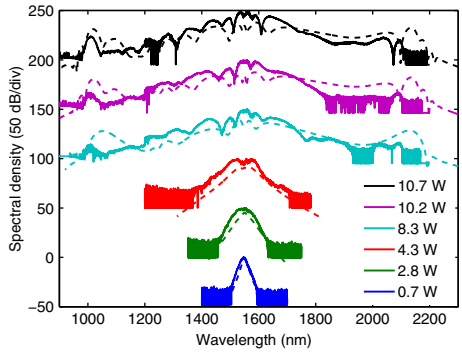

Fig. 4. Buildup of the supercontinuum in the numerical simulations (dotted lines) matches well with the experimental spectra (solid lines); in particular the peak power at which the dispersive waves become observable.

spread enough to overlap with the normal dispersion regime, as can be seen from the dispersion curve for the 700 nm wide waveguide in Fig. 1.

The coherence properties of the supercontinuum generated in our InGaP waveguides were also studied. Experimentally, one way to quantify the coherence is to look at the fringe visibility of the interference between two independent supercontinua generated by two successive pulses of the pulse train [3,20–22]. This method has the advantage that it potentially allows us to quantify the coherence across the entire spectrum of the supercontinuum in a single measurement. Utilizing the same interference setup as was reported in [20], as shown in Fig. 5(a), the coherence was measured in a 200-nm band around the pump. The low power collected at the waveguide output prevents us from accurately measuring the fringe visibility outside this range. Figure 5(a) shows the interference fringes recorded in this experiment. The visibility of the fringes at a given wavelength, defined as $V = (I_{max} - I_{min})/(I_{max} + I_{min})$, where I_{max} and I_{min} are the maxima and minima of the fringes around that wavelength, gives the first-order coherence at that wavelength if the power is equally divided between the two arms of the interferometer. From Fig. 5(b), we can see that the coherence is greater than 90% over the range where it was measured. It should be noted that these measurements were limited by the noise floor of the optical spectrum analyzer. Although we were unable to measure the coherence of the spectrum at the dispersive waves, it has previously been reported in [20] that they can retain a high degree of coherence despite being spectrally disconnected from the pump. It should also be noted that unlike the case in crystalline silicon, the soliton number of the input pulse is not very high here—$N \approx 15$. This is at the edge where coherence of the soliton fission process is known to be preserved [23]. This is in contrast to the case of crystalline silicon [20] where though the input soliton number was high ($N \approx 20$), the coherence was still preserved but only because of two-photon absorption limiting the peak power and thus the number of solitons in the waveguide. In the present case, the nonlinear losses from three-photon and free-carrier absorption are too low for this effect, and hence the input soliton number needs to remain low in order to maintain the coherence. To stress this point, the effect of increasing pulse

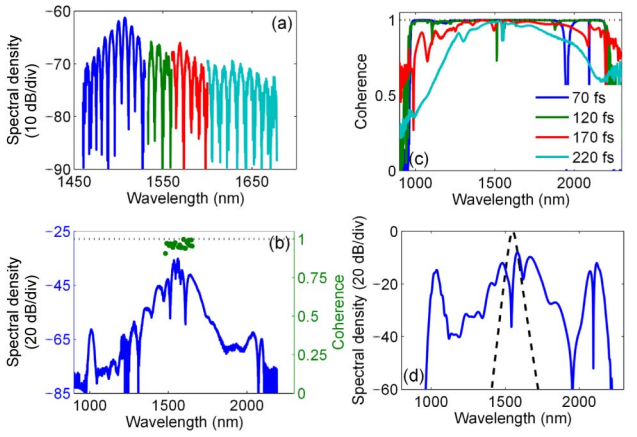

Fig. 5. (a) Observed interference fringes between two successive pulses of the supercontinuum with different colors representing different alignments of the interference setup to optimize the power collected in that part of the spectrum. (b) Coherence of the supercontinuum around the pump wavelength. (c) The coherence properties of the supercontinuum for various input pulse FWHMs ranging from 70 to 220 fs corresponding to soliton numbers 6, 10, 15, and 19, respectively. The degradation of coherence for soliton numbers $N > 15$ is clear. (d) The simulated supercontinuum spectrum (solid line) for the 70-fs input pulse (dotted line) is still octave spanning.

widths (and thus increasing soliton number) on the coherence properties of the supercontinuum is shown in Fig. 5(c). Other simulation parameters including the nonlinear losses were kept the same as in the current experiment. It is clear that beyond a pulsewidth of 170 fs ($N \approx 15$), the coherence indeed degrades dramatically. Figure 5(d) shows the simulated supercontinuum spectrum in the same waveguide generated from a 70-fs pulse with the same peak power thus ensuring that the soliton number is lower ($N \approx 6$). One can see that consequently the coherence is perfect virtually across the entire spectrum, which still spans an octave. Thus, this platform offers a way to efficiently generate a coherent octave-spanning supercontinuum with low pulse energies (<1 pJ) at telecom wavelengths without having to incur large nonlinear losses in order to preserve the coherence.

In conclusion, we have demonstrated the potential of our newly proposed platform for on-chip nonlinear optics by generating an octave-spanning supercontinuum pumped at 1550 nm. Compared to other popular on-chip platforms like silicon-on-insulator, we demonstrate a wider supercontinuum at one order of magnitude lower pulse energies due to a larger value of the nonlinear parameter γ as well as significantly lowered nonlinear losses while still pumping at 1550 nm. Wavelengths below 1100 nm are also accessible due to the larger bandgap of the material compared to silicon. The advantage of using a III-V membrane approach is that it is possible to achieve a large index contrast between the III-V layer and the oxide layer beneath, enabling large intensities to be coupled into the waveguides for nonlinear processes as well as to tailor the dispersion properties for phasematching purposes. Following a similar approach, other groups have also demonstrated interesting nonlinear functionalities [24]. Potentially, the large second-order nonlinear coefficients of III-V materials could be exploited on the same platform. Finally, using this approach, it is also possible to integrate such III-V nonlinear devices with the established platforms like SOI or silicon nitride to exploit the already well-developed functionalities there.

Funding. Belgian Science Policy Office (BELSPO) Interuniversity Attraction Pole (IAP); FP7-ERC-MIRACLE; Special Research Fund (BOF).

REFERENCES

1. A. L. Dobryakov, S. A. Kovalenko, A. Weigel, J. L. Pérez-Lustres, J. Lange, A. Müller, and N. P. Ernsting, Rev. Sci. Instrum. **81**, 113106 (2010).
2. Z. Lijia, X. Xiangjun, L. Bo, W. Yongjun, Y. Jianjun, and Y. Chongxiu, Opt. Express **18**, 15003 (2010).
3. A. R. Johnson, A. S. Mayer, A. Klenner, K. Luke, E. S. Lamb, M. R. E. Lamont, Y. Okawachi, F. W. Wise, M. Lipson, U. Keller, and A. L. Gaeta, *Proc. CLEO* (Optical Society of America, 2015), paper SF2D.1.
4. H. Jung, C. Xiong, K. Y. Fong, X. Zhang, and H. X. Tang, Opt. Lett. **38**, 2810 (2013).
5. H. Sun, K. Wang, R. Salem, P. Fendel, and A. C. Foster, *Proc. CLEO* (Optical Society of America, 2015), paper SM1P.6.
6. B. Kuyken, T. Ideguchi, S. Holzner, M. Yan, T. W. Hänsch, J. Van Campenhout, P. Verheyen, S. Coen, F. Leo, R. Baets, G. Roelkens, and N. Picqué, Nat. Commun. **6**, 6310 (2015).
7. M. R. Lamont, B. Luther-Davies, D. Y. Choi, S. Madden, and B. J. Eggleton, Opt. Express **16**, 14938 (2008).
8. R. Holzwarth, T. Udem, T. W. Hänsch, J. C. Knight, W. J. Wadsworth, and P. S. J. Russell, Phys. Rev. Lett. **85**, 2264 (2000).
9. U. D. Dave, B. Kuyken, F. Leo, S.-P. Gorza, S. Combrie, A. De Rossi, F. Raineri, and G. Roelkens, Opt. Express **23**, 4650 (2015).
10. S. Sauvage, Y. Bernard, I. Sagnes, G. Patriarche, F. Glas, G. Le Roux, M. Bensoussan, and J. A. Levenson, J. Opt. Soc. Am. B **18**, 81 (2001).
11. I. Cristiani, R. Tediosi, L. Tartara, and V. Degiorgio, Opt. Express **12**, 124 (2004).
12. J. M. Dudley, G. Genty, and S. Coen, Rev. Mod. Phys. **78**, 1135 (2006).
13. P. Colman, S. Combrié, G. Lehoucq, A. de Rossi, and S. Trillo, Phys. Rev. Lett. **109**, 093901 (2012).
14. S. Krishnamurthy, Z. G. Yu, L. P. Gonzalez, and S. Guha, J. Appl. Phys. **109**, 033102 (2011).
15. B. R. Bennett, R. A. Soref, and J. A. del Alamo, IEEE J. Sel. Top. Quantum Electron. **26**, 113 (1990).
16. P. Thiagarajan, J. F. Schmerge, C. S. Menoni, M. Marconi, O. E. Martinez, J. J. Rocca, M. J. Hafich, H. Y. Lee, and G. Y. Robinson, Appl. Phys. Lett. **59**, 90 (1991).
17. F. Leo, S.-P. Gorza, J. Safioui, P. Kockaert, S. Coen, U. D. Dave, B. Kuyken, and G. Roelkens, Opt. Lett. **39**, 3623 (2014).
18. F. Leo, J. Safioui, B. Kuyken, G. Roelkens, and S.-P. Gorza, Opt. Express **22**, 28997 (2014).
19. T. Goto, A. Ishizawa, R. Kou, T. Tsuchizawa, N. Matsuda, K. Hitachi, T. Nishikawa, K. Yamada, T. Sogawa, and H. Gotoh, *Proc. CLEO* (Optical Society of America, 2015), paper SW4G.1.
20. F. Leo, S. P. Gorza, S. Coen, B. Kuyken, and G. Roelkens, Opt. Lett. **40**, 123 (2015).
21. M. Bellini and T. W. Hänsch, Opt. Lett. **25**, 1049 (2000).
22. X. Gu, M. Kimmel, A. P. Shreenath, R. Trebino, J. M. Dudley, S. Coen, and R. S. Windeler, Opt. Express **11**, 2697 (2003).
23. E. J. R. Kelleher, M. Erkintalo, and J. C. Travers, Opt. Lett. **37**, 5217 (2012).
24. M. Pu, L. Ottaviano, E. Semenova, L. K. Oxenløwe, and K. Yvind, *Proc. CLEO: 2015 Postdeadline Paper Digest* (Optical Society of America, 2015), paper JTh5A.9.